PERGAMON

International Journal of Rock Mechanics & Mining Sciences 38 (2001) 607–619

International Journal of
Rock Mechanics
and Mining Sciences

www.elsevier.com/locate/ijrmms

Time-dependent closure of a fracture with rough surfaces under constant normal stress

K. Matsuki*, E.Q. Wang[1], K. Sakaguchi, K. Okumura

Department of Geoscience and Technology, Tohoku University, 01 Aramaki-Aza-Aoba, Aoba-ku, Sendai 980-8579, Japan

Accepted 10 April 2001

Abstract

Time-dependent closure of a fracture with rough surfaces subjected to stepwise normal stress was considered theoretically by viscoelastic modeling of rock. A formula for the relationship between constant normal stress and time-dependent closure as a function of time was derived based on the aperture distributions of a fracture and the relaxation modulus $Y_{E'}(t)$ of rock. Theoretical consideration showed that the ultimate closure of a fracture under constant normal stress can be estimated from the normal stress–elastic closure curve by using the values of the relaxation modulus at $t = 0$ and ∞, and that the ultimate time-dependent closure is independent of the normal stress if the elastic closure is linear with the logarithm of the normal stress. Experiments and a Monte Carlo simulation on time-dependent closure under constant normal stress were conducted for a hydraulic fracture created in granite in the laboratory to provide the verification of the theory. The results obtained in the experiments showed that the ultimate time-dependent closure of a hydraulic fracture was almost independent of the normal stress when the elastic closure was linear with the logarithm of the normal stress. A Monte Carlo simulation on time-dependent closure of a fracture under constant normal stress showed that time-dependent closure of a fracture for which the elastic closure is linear with the logarithm of the normal stress does not depend on the normal stress because the increase in contact area during time-dependent closure increases with the normal stress.

1. Introduction

Many researchers in civil and mining engineering have investigated the mechanical properties of discontinuities such as joints in a rock mass [e.g. 1,2], since the mechanical behaviors as well as fluid permeability of a rock mass are governed by such discontinuities. In the field of geothermal energy extraction engineering, an artificial fracture created by hydraulic fracturing is expected to act as a heat exchanger to enhance the production of geothermal energy [3]. In the field of underground nuclear waste disposal, fracture systems in a rock mass could provide a path for radionuclides to be transported into biosphere. In these fields, the evaluation of water flow through natural discontinuities or hydraulically created fractures is essential for designing associated rock structures. While a fracture is closed macroscopically due to rock stresses, an aperture still remains and provides a path for water flow [4–11]. Accordingly, water flow through a fracture is determined by the aperture distribution in a fracture resulting from the stresses.

The two surfaces of a fracture, such as a hydraulic fracture, are more or less related to each other at long wavelengths [12–14]. Thus, a natural fracture which has not been subject to shear deformation is more or less a "mated" fracture, in contrast to an artificial "fracture" with polished surfaces which are completely unrelated below the corner frequency [15]. Accordingly, the statistical and spectral parameters of the aperture of a fracture cannot be estimated in a straightforward manner from those of the fracture surfaces because the aperture distribution depends on the degree of correlation between the height distributions ("matedness") of the fracture surfaces. The closing process under normal stress of a fracture is highly non-linear depending on the matedness of the two surfaces [16]. The non-linearity arises because as normal stress increases the contact area increases, resulting in stiffening the fracture [17]. Thus,

*Corresponding author. Tel.: +81-22-217-7380; fax: +81-22-217-7380.

E-mail addresses: matsuki@rock.earth.tohoku.ac.jp (K. Matsuki), wangerqi@hotmail.com (E.Q. Wang), saka@rock.earth.tohoku.ac.jp (K. Sakaguchi), okumura@rock.earth.tohoku.ac.jp (K. Okumura).

[1] At present Tongji University, China.

1365-1609/01/$ - see front matter
PII: S1365-1609(01)00022-3

closure of a fracture is governed by the aperture distribution in the undeformed state, i.e., by the mismatched part of the fracture surfaces. Goodman [16] reported that no visible damage was observed on the surfaces of a mated fracture after loading. Pyrak-Nolte et al. [17] showed that after repeated cycling, the non-linearity of natural fracture deformation persisted without hysteresis, thus leading to the conclusion that deformation is primarily elastic.

Brown and Scholz [15] developed a theory for simulating the elastic closure of a fracture with rough surfaces under normal stress. They introduced the concept of composite topography of a fracture, and obtained a formula for the relationship between normal stress–elastic closure that is also applicable to a mated fracture. The theory is based on the Hertzian theory of elastic contact [18] and the probabilistic and spectral characterization of the composite topography. The heights of the composite topography are given by the summation of the heights of the two surfaces from each reference plane. The aperture is the rest between the reference planes. If the probability density function (PDF) of the height of the composite topography is Gaussian or inverted chi-square, the relationship between normal stress and elastic closure is obtained by using the power spectral density (PSD) of the height of the composite topography measured across a linear path. Matsuki et al. [19] reproduced elastic closure under normal stress by using the formula of Brown and Scholz for a hydraulic fracture created in granite in the laboratory. They showed that the true contact area increases approximately in proportion to the normal stress, which was also observed experimentally by using a metal-injection technique [17]. For a fracture under both normal and shear stresses, Yoshioka and Scholz [20] proposed a theory for the initial properties of a fracture. However, the theories presented until now are for elastic behaviors caused by the increase in stresses.

Time-dependent closure (or opening) and sliding of a fracture may occur under constant normal and shear stresses since rock is not perfectly elastic [21]. Accordingly, water flow through a fracture may decrease with time due to the normal stress while it may more or less increase with time due to the shear dilation caused by the shear stress [1,2]. Prediction of the long-term closure and sliding of a fracture is necessary for estimating the long-term permeability of a fracture, particularly in the fields of nuclear waste disposal and geothermal energy extraction. In these fields, time-dependent deformation may be accumulated for a long time to result in appreciable changes in the permeability of a rock mass even if the rock is apparently elastic. However, there have been very few investigations on time-dependent behaviors of a fracture with rough surfaces. Accordingly, at present, we cannot predict whether the permeability of a given fracture decreases or increases with time for given values of the normal and shear stresses.

Time-dependent behaviors such as creep, stress relaxation and an elastic strain recovery of rock are often modeled with viscoclasticity by using rheological models [21,22]. In this approach, deformation of rock is simply expressed as a function of time and stresses without referring to the mechanisms behind the time-dependent deformation. The viscoelastic parameters such as relaxation modulus and creep compliance of rock reflect the mechanisms such as subcritical crack growth [23]. Therefore, viscoelastic modeling of rock does not directly mean that rock is assumed to deform due to real viscous flow. This gives us a practical way to estimate time-dependent deformation of rock structures by measuring the viscoelastic parameters of the rock. Lee and Radok [24] showed that the so-called correspondence principle [25] can be applied to the contact of viscoelastic bodies provided that the loading program is such that the contact area is continuously increasing. They analyzed the indentation of a rigid sphere on a plane surface of a viscoelastic half-space. Yang [26] investigated the contact of two linear viscoelastic bodies of arbitrary profile. However, there have been very few investigations of viscoelastic behaviors of a fracture with rough surfaces even for the process of pure closure.

The purpose of this study is to establish a method for estimating long-term closure of a fracture with rough surfaces under constant normal stress. For this purpose, both modeling of time-dependent behaviors of rock and modeling of a fracture are necessary. In the first phase of this paper, the time-dependent closure of a fracture with rough surfaces subjected to a stepwise normal stress was investigated theoretically based upon the viscoelastic contact of asperities on the surfaces. A formula for the relationship between constant normal stress and time-dependent closure as a function of time was derived based on the aperture distribution of the fracture and the relaxation modulus $Y_{E'}(t)$ of rock. The relaxation modulus $Y_{E'}(t)$ is a viscoelastic parameter corresponding to elastic constant $E'(= E/(1-\nu^2))$ in elasticity, where E is Young's modulus and ν is Poisson's ratio. It was shown that the ultimate closure of a fracture under constant normal stress can be estimated from the normal stress–elastic closure curve if the values of the relaxation modulus of rock $Y_{E'}(0)$ and $Y_{E'}(\infty)$ are determined. Furthermore, the ultimate time-dependent closure was shown to be independent of the normal stress if the elastic closure is linear with the logarithm of the normal stress. In the second phase of this paper, time-dependent closure under constant normal stress was measured for a hydraulic fracture created in granite in the laboratory to verify the theory, and was compared to the results of a Monte Carlo simulation on time-dependent closure of a fracture under constant normal stress. The results obtained in the simulation showed

that time-dependent closure of a fracture does not depend on the normal stress if the elastic closure is linear with the logarithm of the normal stress because the increase in contact area during time-dependent closure increases with the normal stress.

2. Theory of time-dependent closure

2.1. Hertzian theory of two elastic spheres in contact

Consider two elastic spheres of radius R_1 and R_2 in contact (Fig. 1). Isotropy is assumed throughout this paper. If the two spheres are made of the same material with bulk modulus K and shear modulus (rigidity) G, the constitutive law is given by

$$\sigma_m = 3K\varepsilon_m, \quad s_{ij} = 2Ge_{ij}, \tag{1}$$

where σ_m and ε_m are the mean normal stress and mean normal strain, respectively, and s_{ij} and e_{ij} are the stress deviation and strain deviation, respectively, defined as

$$s_{ij} = \sigma_{ij} - \delta_{ij}\frac{\sigma_{kk}}{3}, \quad e_{ij} = \varepsilon_{ij} - \delta_{ij}\frac{\varepsilon_{kk}}{3}, \tag{2}$$

where δ_{ij} is the Kronecker delta. In these equations, the usual summation convention for the tensor suffix notation is assumed. The elastic constants K and G are related to Young's modulus E and Poisson's ratio v by [21]

$$E = \frac{9KG}{3K+G}, \quad v = \frac{3K-G}{2(3K+G)}. \tag{3}$$

Assuming that deformation is small, the relationships among the radius a of the circular contact area, the displacement δ between the two spheres (hereafter referred to as closure) and the load P are given by [18]

$$a^2 = \beta\delta \tag{4}$$

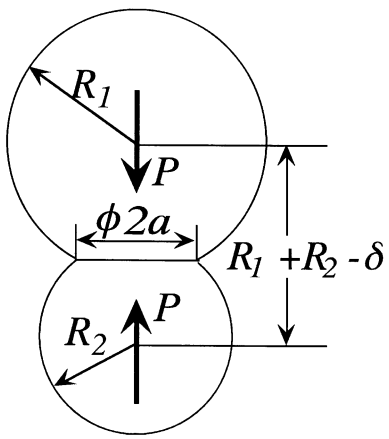

Fig. 1. Notations in the Hertzian contact of two elastic spheres.

and

$$P = \frac{2E'a^3}{3\beta} = \frac{2\beta^{1/2}E'\delta^{3/2}}{3}, \tag{5}$$

where

$$\frac{1}{\beta} = \frac{1}{R_1} + \frac{1}{R_2} \tag{6}$$

and

$$\frac{1}{E'} = \frac{1-v^2}{E} = \frac{3K+4G}{2G(6K+2G)}. \tag{7}$$

Eq. (4) is derived from the geometrical relationship between a and δ. The elastic constant E' can be determined experimentally, for example, by indentation of a rigid cylinder of radius R on a half-space of rock (a plane surface of a block with sufficiently large dimensions). The load F is related to the indentation u by [18]

$$F = 2RE'u. \tag{8}$$

2.2. Two viscoelastic spheres in contact

Let us consider the contact of two linear viscoelastic spheres with the same dimensions as in the elastic case described above. The constitutive law of a linear viscoelastic material is given in the Laplace domain as [25]

$$\bar{\sigma}_m = \frac{Q_V(s)}{P_V(s)}\bar{\varepsilon}_m, \quad \bar{s}_{ij} = \frac{Q_s(s)}{P_s(s)}\bar{e}_{ij}, \tag{9}$$

where $Q_V(s)$, $P_V(s)$, $Q_s(s)$ and $P_s(s)$ are polynomials of s, the parameter in the Laplace transformation, and an upper bar means the Laplace transform of the function. The suffixes V and S indicate volumetric and shear modes, respectively. Comparison of Eq. (9) with Eq. (1) shows that the elastic constants $3K$ and $2G$ correspond to the viscoelastic parameters Q_V/P_V and Q_S/P_S in the Laplace domain, respectively. This gives a basis for the so called correspondence principle [25]. The correspondence principle says that the solution for a linear viscoelastic material can be obtained in the Laplace transform by replacing $3K$ and $2G$ in the corresponding linear elastic solution with the same boundary conditions by Q_V/P_V and Q_S/P_S, respectively, and the actual loading condition by the Laplace transform.

The constitutive law given by Eq. (9) can be expressed with the relaxation moduli $\bar{Y}_V$ and $\bar{Y}_S$. The relaxation modulus is the change in stress with time when a unit of the corresponding strain is increased in a stepwise manner. Thus, the following relationships are obtained [25]

$$\frac{Q_V}{P_V} = s\bar{Y}_V, \quad \frac{Q_S}{P_S} = s\bar{Y}_S. \tag{10}$$

From Eqs. (7), (9) and (10), the relaxation modulus $\bar{Y}_{E'}$, which corresponds to E' in elasticity, is given in the

Laplace domain by

$$\bar{Y}_{E'} = \frac{\bar{Y}_S(2\bar{Y}_V + \bar{Y}_S)}{\bar{Y}_V + 2\bar{Y}_S}. \tag{11}$$

$Y_{E'}(t)$ can be determined experimentally by measuring the change in load $F(t)$ with time when a rigid cylinder of radius R is indented on a plane surface by u_0 in a stepwise manner. By using the correspondence principle for the elastic solution of Eq. (8), the Laplace transform of Eq. (8) is

$$\bar{F} = 2R\bar{Y}_{E'}u_0. \tag{12}$$

Accordingly, $Y_{E'}(t)$ is determined by an inverse Laplace transformation of the above equation as

$$Y_{E'}(t) = \frac{F(t)}{2Ru_0}. \tag{13}$$

$Y_{E'}(t)$ is usually a monotonically decreasing function of time, and may approach a constant value $Y_{E'}(\infty)$ at infinite time. $Y_{E'}(0)$ is the contribution of the elastic components and is equal to E'. Thus, viscoelasticity in the contact problem is expressed with the single viscoelastic parameter $Y_{E'}(t)$.

In the viscoelastic contact of a fracture with rough surfaces under a constant load, the load or pressure produced by the initial elastic contact on each contact area is never constant, but decreases with time because the contact area that supports a constant total load increases with time due to the time-dependent closure. However, the closure of a fracture increases monotonously with time, so both the closure and the contact area of each contact point, which is expressed with two spheres in contact in this study, increase monotonously. Accordingly, the correspondence principle can be applied to obtain closure of two viscoelastic spheres in contact from the corresponding elastic solution, whereas the boundary conditions change with time [24]. In the case of cyclic loading or opening of a fracture, the decrease in contact area occurs and therefore it is difficult to obtain the viscoelastic behaviors of two bodies in contact because the correspondence principle cannot be applied to the case.

The relationship between the radius of the contact area $a(t)$ and the closure $\delta(t)$ for two viscoelastic spheres in contact is given by the same equation as (4) because this is derived from their geometrical relationship. Thus

$$a^2(t) = \beta\delta(t). \tag{14}$$

By using the correspondence principle for the elastic solution given by Eq. (5), the load $P(t)$ is obtained in the Laplace domain as

$$\bar{P} = \frac{2}{3\beta}s\bar{Y}_{E'}\overline{a^3}. \tag{15}$$

By an inverse Laplace transformation of the above equation, we have the load $P(t)$ as a function of time.

$$P(t) = \frac{2}{3\beta}\int_0^t Y_{E'}(t-\xi)\frac{da^3(\xi)}{d\xi}d\xi + \frac{2}{3\beta}a^3(0)Y_{E'}(t), \tag{16}$$

where $a(0)$ is the radius of the contact area at $t = 0$. The second term on the right-hand side expresses the relaxation of the initial elastic load $P(0)$, and the hereditary integral of the first term expresses the contribution of the increase in the contact area. Therefore, if no contact occurs at $t = 0$, we do not have the second term on the right-hand side and the hereditary integral should start at the onset of contact.

From Eq. (14), $a(\xi)$ in Eq. (16) is replaced by $\delta(\xi)$ as

$$P(t) = \beta^{1/2}\int_0^t Y_{E'}(t-\xi)[\delta(\xi)]^{1/2}\frac{d\delta(\xi)}{d\xi}d\xi + P(0)\frac{Y_{E'}(t)}{Y_{E'}(0)}, \tag{17}$$

where the initial elastic load $P(0)$ is given by

$$P(0) = \frac{2E'\beta^{1/2}}{3}[\delta(0)]^{3/2}. \tag{18}$$

In the above equation, $Y_{E'}(0)$ is replaced by the elastic constant E'. Thus, Eq. (18) coincides with Eq. (5).

2.3. Time-dependent closure of a fracture

Now consider a fracture with a number of local summits on its composite topography, in which the ith local summit of height z_i has a local minimum aperture of u_{mi} and a radius β_i (Fig. 2). Let us denote the closure of a fracture as $\Delta(t)$. We assume that a fracture is initially in contact at a single point. When the closure of a fracture in a stepwise manner at $t = 0$ is given as $\Delta(0)$, local minimum apertures of u_{mi} smaller than $\Delta(0)$ are in contact and produce an instantaneous elastic load P_0, which is then kept constant. When the fracture is closed by $\Delta(t)$, a local minimum aperture of u_{mi} smaller than $\Delta(t)$ is closed by

$$\delta_i(t) = \Delta(t) - u_{mi}. \tag{19}$$

The contact of a local minimum aperture of u_{mi} greater than $\Delta(0)$ occurs at $t = t_{ci}$ when the following condition

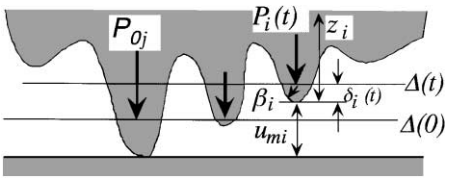

Fig. 2. Elastic and time-dependent closure of a composite topography of a fracture. The ith local summit has a local minimum aperture of u_{mi} and a radius β_i. $\Delta(0)$ is an instantaneous closure and produces an instantaneous load P_{0j}, etc. With a closure $\Delta(t)$, the ith local minimum aperture is closed by $\delta_i(t)$ and produces a time-dependent load $P_i(t)$.

is satisfied:

$$\Delta(t_{ci}) = u_{mi}, \tag{20}$$

where t_{ci} is zero if $u_{mi} \leqslant$ to $\Delta(0)$.

The instantaneous elastic load P_0 is obtained by summing the elastic load P_{0i} given by Eq. (18) for each local minimum aperture of u_{mi} smaller than $\Delta(0)$

$$P_0 = \sum_{u_{mi}<\Delta(0)} P_{0i} = \frac{2E'}{3} \sum_{u_{mi}<\Delta(0)} \beta_i^{1/2} [\Delta(0) - u_{mi}]^{3/2}. \tag{21}$$

If a unit of nominal fracture area is considered, the load is equivalent to the normal stress. This normal stress can also be determined statistically using the formula of Brown and Scholz [15]

$$\sigma_0 = \frac{2E'}{3} \eta \int_0^{\Delta} \left[\int \beta^{1/2} B(\beta/u_m)\, d\beta \right] (\Delta - u_m)^{3/2} \phi(u_m)\, du_m, \tag{22}$$

where u_m is the magnitude of the local minimum apertures, η is the number of local minimum apertures (summits on the composite topography) in a unit area, $\phi(u_m)$ is the PDF of the local minimum apertures, $B(\beta/u_m)$ is the conditional PDF of the radius of the local minimum apertures, and $\Delta(=\Delta(0))$ is the closure of the fracture. This equation is obtained by rewriting the original formula with the term for the local minimum aperture and by assuming that the mean value of the tangential stress correction factor is 1 (see [15]). The functions $\phi(u_m)$, $B(\beta/u_m)$ and the parameter η are obtained by the aperture PSD in a linear profile and the aperture PDF, if the PDF is given by a Gaussian [27] or χ^2 distribution [28]. Clearly, Eq. (21) is another expression of Eq. (22) provided that β_i and u_{mi} are distributed according to their PDFs.

For a local minimum aperture in contact at $t = 0$, the load $P_i(t)$ for $t > 0$ is determined by replacing $\delta(t)$ in Eq. (17) by Eq. (19).

$$P_i(t) = \beta_i^{1/2} \int_0^t Y_{E'}(t-\xi)[\Delta(\xi) - u_{mi}]^{\frac{1}{2}} \frac{d\Delta(\xi)}{d\xi} d\xi + P_{0i} \frac{Y_{E'}(t)}{Y_{E'}(0)}. \tag{23}$$

For a local minimum aperture of u_{mi} greater than $\Delta(0)$, the load $P_i(t)$ is given by the following equation when $t > t_{ci}$:

$$P_i(t) = \beta_i^{1/2} \int_{t_{ci}}^t Y_{E'}(t-\xi)[\Delta(\xi) - u_{mi}]^{1/2} \frac{d\Delta(\xi)}{d\xi} d\xi. \tag{24}$$

Since $t_{ci} = 0$ for the local minima apertures in contact at $t = 0$, the relationship between a constant normal load P_0 and closure of the fracture $\Delta(t)$ is finally given by

$$P_0 = \sum_{t \geqslant t_{ci}} \beta_i^{1/2} \int_{t_{ci}}^t Y_{E'}(t-\xi)[\Delta(\xi) - u_{mi}]^{1/2} \frac{d\Delta(\xi)}{d\xi} d\xi + P_0 \frac{Y_{E'}(t)}{Y_{E'}(0)}. \tag{25}$$

This equation means that the relaxation of the initial elastic load given by the second term on the right-hand side is compensated by the first term to keep the total load constant. The first term expresses the effects of the increase in the closure and, accordingly, those of the increase in the contact area. This formula is applicable to both a mated fracture and a non-mated fracture if the PDF of u_{mi} and the conditional PDF of β_i are given. From Eqs. (14) and (19), the contact area as a function of time $A_c(t)$ is given by

$$A_c(t) = \pi \sum_{u_{mi}<\Delta(t)} \beta_i [\Delta(t) - u_{mi}]. \tag{26}$$

3. Ultimate closure of a fracture

Eq. (25) does not explicitly give the closure of a fracture $\Delta(t)$ as a function of time because the closure of a fracture and the time when each local minimum aperture is initially in contact are related to each other. That is, the closure of a fracture depends on the history of the contact area and vice versa. Therefore, to determine closure as a function of time for a given constant normal stress, we have to take a numerical approach by modeling a fracture with the distributions of local minimum aperture and its radius, as will be described later. However, the ultimate value $\Delta(\infty)$ of the closure can be derived using the ultimate value $Y_{E'}(\infty)$ of the relaxation modulus.

In Eq. (25), the value P_0—the second term on the right-hand side is $P_0(1 - Y_{E'}(\infty)/Y_{E'}(0))$ at $t =$ infinity, which is finite and less than P_0. Therefore, $\Delta(\infty)$ must be a constant because the hereditary integral in Eq. (25) must be finite for $t =$ infinity, unless $Y_{E'}(\infty)$ is zero, which is not likely for hard rocks as far as an engineering problem is concerned. Thus, in Eq. (25), at $t =$ infinity, $d\Delta(\xi)/d\xi$ is zero and $Y_{E'}(t-\xi)$ is $Y_{E'}(\infty)$ regardless of ξ. As a result, by carrying out the integral and by using Eq. (21), $\Delta(\infty)$ is obtained as

$$P_0 = \frac{2Y_{E'}(\infty)}{3} \sum_{u_{mi}<\Delta(\infty)} \beta_i^{1/2} [\Delta(\infty) - u_{mi}]^{3/2}. \tag{27}$$

Comparison of Eq. (27) with Eq. (21) indicates that $\Delta(\infty)$ is closure given by the elastic contact of the same fracture under the same load, but the elastic component of the relaxation modulus is $Y_{E'}(\infty)$, which is less than $Y_{E'}(0)$. At $t =$ infinity, the effects of viscous elements, usually expressed with dashpots, disappear, and the mechanical behaviors of a viscoelastic material can be

completely described by the remaining elastic elements with elastic modulus $Y_{E'}(\infty)$ (see the appendix for details). Eq. (27) can be written as

$$\frac{Y_{E'}(0)}{Y_{E'}(\infty)}P_0 = \frac{2Y_{E'}(0)}{3}\sum_{u_{mi}<\Delta(\infty)}\beta_i^{1/2}[\Delta(\infty)-u_{mi}]^{3/2}. \quad (28)$$

This equation means that the ultimate closure $\Delta(\infty)$ of a fracture subjected to a constant normal load of P_0 is given by elastic closure when the fracture is subjected to a load of $P_0 Y_{E'}(0)/Y_{E'}(\infty)$, which is greater than P_0. Therefore, if a normal stress–elastic closure curve is given for a fracture and if the ratio of $Y_{E'}(0)/Y_{E'}(\infty)$ is determined, the ultimate closure $\Delta(\infty)$ of a fracture can be determined from the curve of elastic closure, as shown in Fig. 3. This gives us a useful tool for estimating the ultimate closure of a fracture since the ultimate closure of a different fracture in a rock mass can be estimated by the elastic closure once the relaxation modulus $Y_{E'}(t)$ is determined for the rock.

If the elastic closure Δ is linear versus the logarithm of normal stress σ_n [16] as

$$\Delta = A + B\ln\sigma_n, \quad (29)$$

where A and B are constants, the ultimate time-dependent closure $(\Delta(\infty)-\Delta(0))$ is

$$\Delta(\infty)-\Delta(0) = B\ln\frac{Y_{E'}(0)}{Y_{E'}(\infty)}. \quad (30)$$

This equation shows that the ultimate time-dependent closure is independent of the normal stress if the Goodman's relation (Eq. (29)) gives the elastic closure (hereafter the fracture for which the elastic closure is given in the form of Eq. (29) is called Goodman's fracture). This independence of the ultimate time-dependent closure of a Goodman's fracture of the normal stress is quite different from behaviors of an intact specimen, for which time-dependent displacement under compression increases with the axial stress [21]. Obviously, a fracture for which the elastic closure does not obey the Goodman's relation should not show this independence. As mentioned previously, the contact area in elastic loading increases approximately in proportion to the normal stress [17,19]. This means that the contact area of a Goodman's fracture increases in an accelerated manner with regard to the closure (see Fig. 3, which satisfies Eq. (29)). Therefore, the same increase in the contact area also occurs for the time-dependent closure of the Goodman's fracture. Accordingly, it can be said that the ultimate time-dependent closure of a Goodman's fracture is independent of the normal stress because the contact area during the time-dependent closure increases with the normal stress. The mechanism for this independence will be further discussed later, referring to the results of a Monte Carlo simulation.

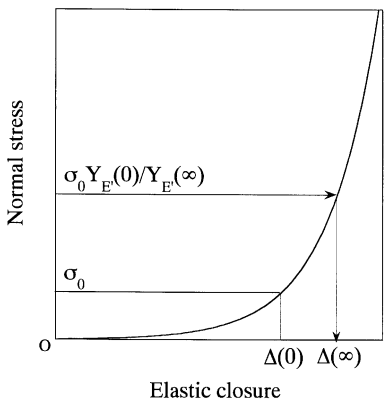

Fig. 3. Determination of ultimate closure of a fracture from the normal stress–elastic closure curve.

4. Experiments

4.1. Hydraulic fracture

Inada granite, quarried at lbaraki prefecture, Japan, was used in the experiments. The mechanical and physical properties are summarized in Table 1. The loading axis for the mechanical properties was perpendicular to the rift plane and the average values determined from five specimens were shown in the table. The diameter of the sample was 35 mm for both uniaxial compression and uniaxial tension while the height was 88 mm for uniaxial compression and 105 mm for uniaxial tension. The elastic modulus E' determined under uniaxial compression was 74.3 GPa.

Hydraulic fracturing was carried out in the laboratory for a block of granite (150 mm × 150 mm × 250 mm) as shown in Fig. 4. A straddle packer was inserted into a central hole, 10 mm diameter, and internal pressure was applied to create a fracture. An axial stress of about

Table 1
Mechanical and physical properties of Inada granite[a]

Uniaxial compressive strength (MPa)	Uniaxial tensile strength (MPa)	Young's modulus[b] (GPa)	Poisson's ratio	Specific gravity	Porosity (%)
163	5.82	71.3	0.2	2.64	0.56

[a] Mechanical properties were measured by applying the load perpendicular to rift plane.
[b] Tangential Young's modulus at 50% of uniaxial compressive strength.

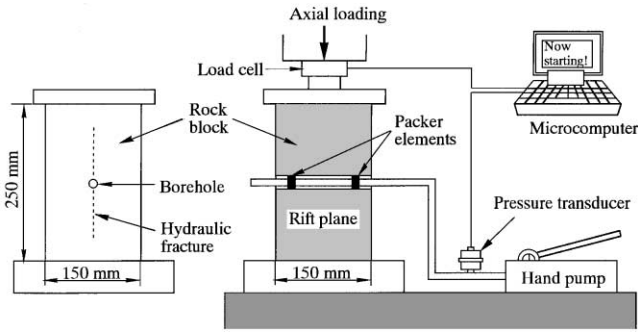

Fig. 4. Hydraulic fracturing system in a block of granite.

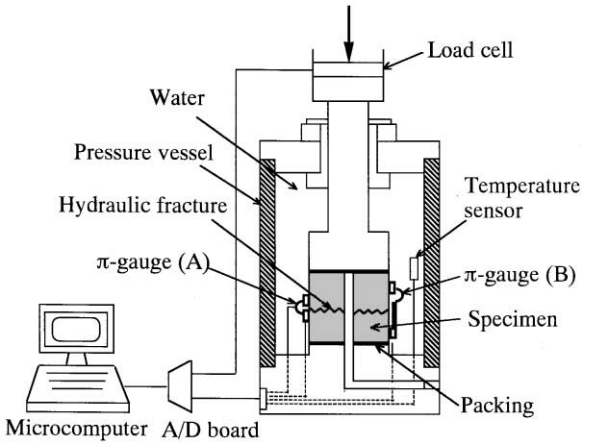

Fig. 5. Testing apparatus for measuring time-dependent closure of a fracture under constant normal stress.

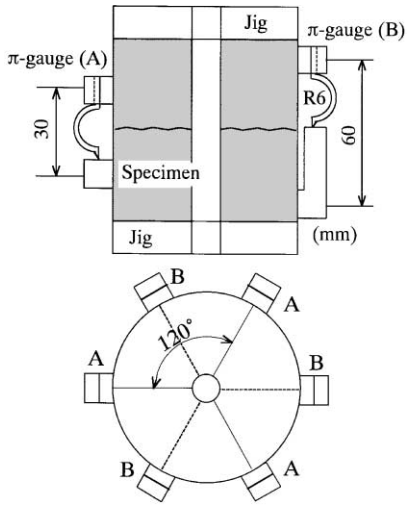

Fig. 6. Two types of π-gauges for measuring closure of a fracture.

3 MPa was applied at the same time to propagate the fracture parallel to the loading axis, which was parallel to the rift plane. Hydraulic fracturing was performed twice changing the distance between the packer elements to obtain a fracture as large as possible. To avoid damaging the fracture surfaces in taking a core from the block, a hole 10 mm in diameter was drilled perpendicular to the fracture plane at a distance about 40 mm from the inner wall of the central hole. Then, a bolt was inserted in the hole, to lightly compress the fracture with nuts during the coring process. The hole served as a central outlet for water in later experiments on permeability, which will not be described in this paper. All four specimens of a hollow cylinder, 66.6 mm in outer diameter, 10 mm in inner diameter and 80 mm in height, were taken from different blocks, and were fixed with glue in a jig. The jig provided reference planes to match the paths for measuring the heights of the two surfaces to obtain the aperture distribution [11]. Since the two surfaces of the fracture were not separated, i.e., the fracture existed in a so-called process zone [23,29], the fracture surfaces were pulled out by applying a uniaxial tensile stress. The residual tensile strength was only 2.1–5.4% of the uniaxial tensile strength of the intact specimen.

The heights of the two fracture surfaces were measured along matched paths in an area of 41 mm × 41 mm using a profilometer with a stylus of 0.025 mm in tip radius to determine the aperture distributions. The interval was 0.01 mm in the direction of the macroscopic fracture growth and 0.1 mm in the perpendicular direction. From the measured data, the aperture PDF was determined and the power spectral density (PSD) of the aperture was calculated for these specimens using a standard FFT (Fast Fourier Transform).

4.2. Experimental method

Fig. 5 shows a system for measuring the closure of a fracture under a constant normal stress. A normal stress of 10–25 MPa was applied to the specimen at a rate of 0.13 MPa/s, and then kept constant. Since the permeability of the fracture was measured at the same time (not described here), the specimen was set in a pressure vessel filled with pure water. The displacements across the fracture were measured using two sets, called A and B, of strain-gauge type π-gauges (Fig. 6). Each set had three π-gauges spaced at 120° around the circumference of the fracture. The effective lengths of the sets A and B were 30 mm and 60 mm, respectively. Accordingly, the difference between the average displacements measured with each set gives the displacement of the intact part 30 mm long, which was removed from the average displacement measured with the set A to obtain the closure of the fracture. The error in the measurement of the displacement was estimated from the scatter in the data to be within ±0.0015 mm. The temperature of the water in the pressure vessel was measured and used to

correct for the effects of temperature on displacement. The data were recorded using a microcomputer. In the initial elastic loading, the data were measured every a half second, and after the normal stress was constant, the data were measured at appropriate intervals until approximately no appreciable increase in displacement was observed. As a result, the measurement was conducted for about 4 days, which may be too short for discussing the long-term closure of the fracture. However, we did not continue the measurement longer because main purpose of this study is to establish a method for estimating long-term closure of a fracture, as described previously.

4.3. Experimental results

Fig. 7 shows the results of the initial elastic loading, a normal stress–elastic closure curve, for each maximum (constant) normal stress. The origin of this figure was set at a normal stress of 57.6 kPa. Different curves were obtained among the specimens. Asperities (apertures) that contributed to small normal stress may be distributed differently in these specimens, resulting in different closures under small normal stresses. A small number of very sharp asperities may cause a quite different initial closure. However, if the curves for constant normal stresses greater than 10 MPa are shifted along the axis of closure to that of a normal stress of 10 MPa, these curves approximately coincide with each other as shown in Fig. 8, although the curve for 20 MPa is still different from the others. This indicates that the fracture surfaces for a normal stress of 20 MPa have different characteristics from the others, probably due to the heterogeneity of the rock. Actually, the increase rate of the normal stress with regard to the closure is much

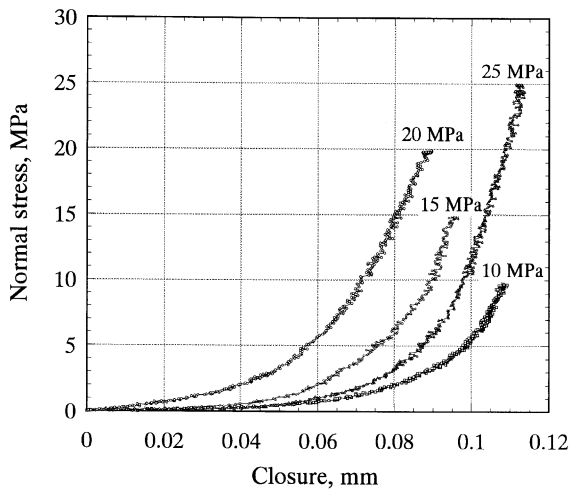

Fig. 7. Normal stress–elastic closure curves of a hydraulic fracture in granite with each maximum (constant) normal stress.

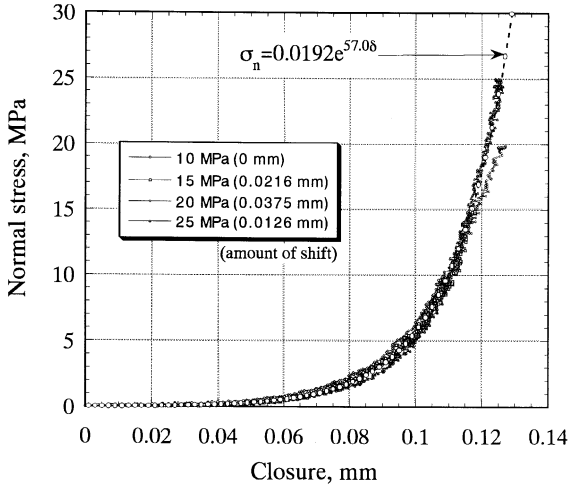

Fig. 8. Normal stress–elastic closure curves when the curves in Fig. 7 for constant normal stress greater than 10 MPa are shifted to the curve for that of 10 MPa. The amount of shift is shown in the figure. The broken curve with open circles is the result of least-squares fitting of Eq. (29).

smaller for a fracture with a normal stress of 20 MPa than that for the others at normal stresses greater than 5 MPa. This suggests that the contact area of a fracture with a normal stress of 20 MPa did not increase with the closure as that of the others did.

To obtain a representative normal stress–elastic closure curve, Goodman's relation [16] (Eq. (29)) was fitted to the data shown in Fig. 8 excluding those for a normal stress of 20 MPa. Using a least-squares method, the following relationship between normal stress σ_n (MPa) and closure δ (mm) was obtained

$$\sigma_n = 0.0192 \exp(57.0\delta). \quad (31)$$

This relationship is also shown in Fig. 8 with open circles. The relationship lies on the experimental data for normal stresses of 10, 15 and 25 MPa. Therefore, the fractures with normal stresses of 10, 15 and 25 MPa are Goodman's fractures while that with a normal stress of 20 MPa is not so. Accordingly, the time-dependent closures of these hydraulic fractures, except that with a normal stress of 20 MPa, are expected to be independent of the normal stress, as described previously.

The time-dependent closure of the fracture under different constant normal stresses is shown in Fig. 9. The time-dependent closure increased to reach an approximately constant value after about 50 h. The ultimate time-dependent closure was similar and did not depend on the normal stress, except that with a normal stress of 20 MPa, which was greater than the others. The reason why the ultimate time-dependent closure of a fracture with a normal stress of 20 MPa, which is not a Goodman's fracture, was greater than that of the others is that the contact area of the fracture did not increase as much as that of the others did during the

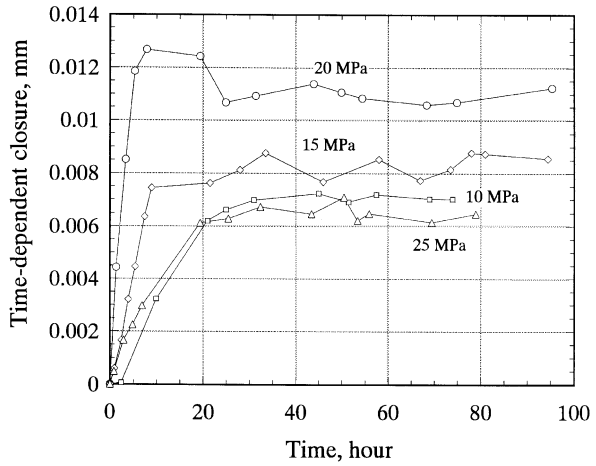

Fig. 9. Time-dependent closure of a hydraulic fracture in granite at constant normal stresses.

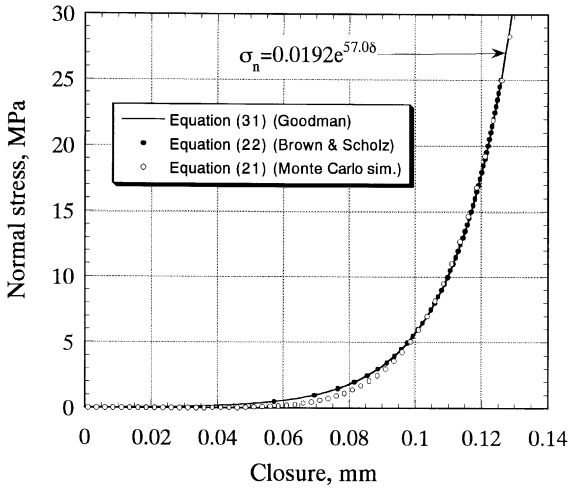

Fig. 10. Comparison of the normal stress–elastic closure curves obtained by fitting Goodman's relation (Eq. (31)), by the formula of Brown and Scholz (Eq. (22)) and by the simulation (Eq. (21)).

time-dependent closure. This exception will be further discussed later. Thus, the experimental results were consistent with the theory presented in the first phase of this paper. The obtained ultimate time-dependent closure was small: less than 12 μm at normal stresses up to 25 MPa. This is because the rock is relatively hard. Larger ultimate time-dependent closure may occur for a less mated (or sheared) fracture in softer rocks. Furthermore, if the closure had been measured longer, the ultimate closure might be greater because the elements with greater time constants (relaxation times) might become effective.

5. Simulation of time-dependent closure of a fracture

5.1. Modeling of a fracture

As mentioned previously, the closure $\Delta(t)$ of a fracture as a function of time cannot be given explicitly for a given normal stress from Eq. (25). Therefore, it is difficult to use the statistical approach taken by Brown and Scholz [15] for elastic contact, to determine time-dependent closure. In this paper, to illustrate time-dependent closure of a fracture and to understand the mechanism for the independence of time-dependent closure of a Goodman's fracture of the normal stress, a Monte Carlo simulation was performed according to Eq. (25). For that purpose, a fracture was modeled with the distributions of local minimum aperture and its radius as briefly described below (see [15,19] for details).

First of all, a fracture model used in simulating time-dependent closure must reproduce the elastic closure obtained experimentally (Fig. 8 and Eq. (31)). As described previously, elastic closure can be estimated by Eq. (22) (the formula of Brown and Scholz) if the PSD of aperture are given and if the aperture PDF is Gaussian or χ^2. Using the measured PSD for a normal stress of 10 MPa, we determined the parameters of a χ^2 distribution for aperture PDF so that the representative normal stress–elastic closure curve obtained in the experiment (Eq. (31)) could be reproduced according to Eq. (22). Fig. 10 shows the simulated relationship, which reproduced Eq. (31) well.

By using the parameters determined, local minima of apertures of magnitude according to $\phi(u_m)$ and radius according to $B(\beta/u_m)$ were generated by a Monte Carlo simulation. Four hundred thousand sets of local minima of apertures and their radii were generated for local minima of apertures less than 0.14 mm. The relationship determined according to Eq. (21) by using the simulation model is also shown in Fig. 10. This relationship is slightly different from the theoretical one at small normal stresses. The increase in the number of local minimum aperture may reduce the difference. However, we did not do this because a huge number of local minima of apertures are necessary to improve the relationship since the aperture PDF is very small for small apertures.

5.2. Simulation of time-dependent closure

Now time-dependent closure of a fracture under constant normal stress can be simulated by using the fracture model that reproduces the elastic closure obtained in the experiment. The relaxation modulus ($Y_{E'}(t)$) was expressed using a three-element model for both volumetric and shear modes (Fig. 11) since we did not measure it directly. The derivation of relaxation modulus for the three-element model is given in the appendix. The relaxation modulus used in the simulation was determined so that the result approximately fits the experimental results of time-dependent closure for a normal stress of 10 MPa (Fig. 9). We used the following

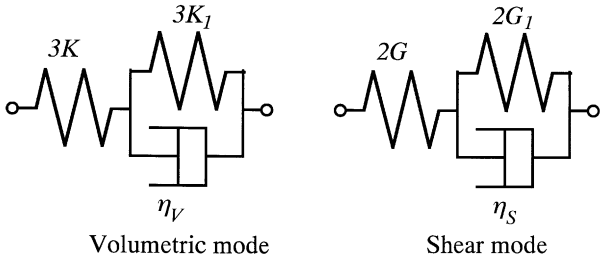

Fig. 11. Three-element model for volumetric and shear modes used in the simulation.

values to obtain the relaxation modulus normalized by E': $K_1/K = G_1/G = 2.0$, $\tau_V = 20$ h and $\tau_S = 30$ h, where τ_V and τ_S are the relaxation times for each mode and are given by $\eta_V/3K_1$ and $\eta_S/2G_1$, respectively. The relaxation modulus normalized by E', used in the simulation, is shown in Fig. 12.

Time-dependent closure was simulated by rewriting Eq. (25) in the form of a finite difference [30]. After determining the instantaneous load P_0 for a given stepwise closure $\Delta(0)$ according to Eq. (21), the closure $\Delta(t)$ at each step of time was determined. Let us consider how to determine the closure at the nth step of time $t_n (t_n = n\Delta t)$. Eq. (25) is given by the summation of the partial integrals.

$$P_0 - P_0\frac{Y_{E'}(t_n)}{Y_{E'}(0)} = \sum_{t \geqslant t_{ci}} \beta_i^{1/2} \times \left[\int_{t_{ci}}^{t_{i_1}} g(\xi)\mathrm{d}\xi + \sum_{j=i_1}^{n-2}\int_{t_j}^{t_{j+1}} g(\xi)\mathrm{d}\xi + \int_{t_{n-1}}^{t_n} g(\xi)\,\mathrm{d}\xi\right], \tag{32}$$

where t_{i_1} is the next step of time closest to the t_{ci}, and

$$g(\xi) = Y_{E'}(t_n - \xi)[\Delta(\xi) - u_{mi}]^{1/2}\frac{\mathrm{d}\Delta(\xi)}{\mathrm{d}\xi}. \tag{33}$$

By using a finite difference form of $\mathrm{d}\Delta(\xi)/\mathrm{d}\xi$ as

$$\frac{\mathrm{d}\Delta(\xi)}{\mathrm{d}\xi} \approx \frac{3\Delta_j - 4\Delta_{j-1} + \Delta_{j-2}}{2\Delta\xi} = \frac{\mathrm{d}\Delta_j}{\Delta\xi} \tag{34}$$

and by assuming the relationship between closure and time is linear for contact in the middle time steps,

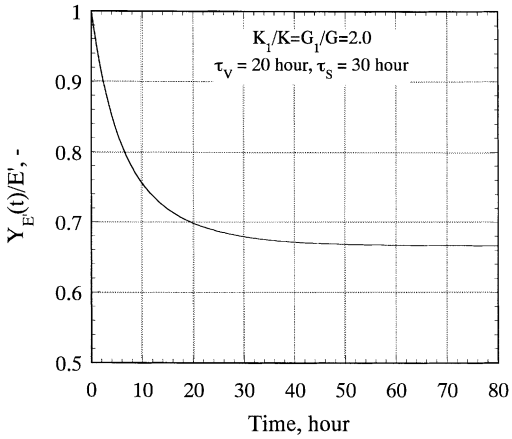

Fig. 12. Relaxation modulus $Y_{E'}(t)$ normalized by E' used in the simulation.

Eq. (32) is written as

$$P_0 - P_0\frac{Y_{E'}(t_n)}{Y_{E'}(0)} = \sum_{u_{mi} < \Delta(t_{n-1})} \beta_i^{1/2}\left[I_{i_1} + \sum_{j=i_1}^{n-2} I_j + I_{n-1}\right] + \sum_{\Delta(t_{n-1}) < u_{mk} < \Delta(t_n)} \beta_k^{1/2} I_k, \tag{35}$$

where

$$I_{i_1} = \frac{Y_{E'}(t_{n-i_1})[\Delta(t_{i_1}) - u_{mi}]^{1/2}\mathrm{d}\Delta_{i_1}}{2}\frac{\Delta(t_{i_1}) - u_{mi}}{\Delta(t_{i_1}) - \Delta(t_{i_1-1})},$$

$$I_j = \frac{Y_{E'}(t_{n-j})[\Delta(t_j) - u_{mi}]^{1/2}\mathrm{d}\Delta_j + Y_{E'}(t_{n-j-1})[\Delta(t_{j+1}) - u_{mi}]^{1/2}\mathrm{d}\Delta_{j+1}}{2},$$

$$I_{n-1} = \frac{Y_{E'}(t_1)[\Delta(t_{n-1}) - u_{mi}]^{1/2}\mathrm{d}\Delta_{n-1} + Y_{E'}(t_0)[\Delta(t_n) - u_{mi}]^{1/2}[3\Delta(t_n) - 4\Delta(t_{n-1}) + \Delta(t_{n-2})]}{2},$$

$$I_k = \frac{3Y_{E'}(t_0)[\Delta(t_n) - u_{mk}]^{1/2}[3\Delta(t_n) - 4\Delta(t_{n-1}) + \Delta(t_{n-2})]}{8[\Delta(t_n) - \Delta(t_{n-1})]} + \frac{Y_{E'}(t_0)[\Delta(t_n) - u_{mk}]^{1/2}[\Delta(t_{n-1}) - \Delta(t_{n-2})]}{4[\Delta(t_n) - \Delta(t_{n-1})]^2}. \tag{36}$$

In the above equation, I_{i_1}, is the integral from the first contact to the next step of time, I_j, is that between the neighboring time steps, I_{n-1} is that for the contact between time steps t_{n-1} and t_n, and I_k is that for the new contact between time steps t_{n-1} and t_n. Eq. (35) is a nonlinear equation of unknown closure $\Delta(t_n)$. Therefore, iteration was conducted to determine $\Delta(t_n)$ using the Newton–Raphson method until the error of $\Delta(t_n)$ was within 0.00001 mm.

To understand the mechanism for the independence of ultimate time-dependent closure of the normal stress, the contact area as a function of time $A_c(t)$ was also calculated by using Eq. (26).

5.3. Results of the simulation

The time-dependent closure obtained in the simulation is shown in Fig. 13 together with the experimental

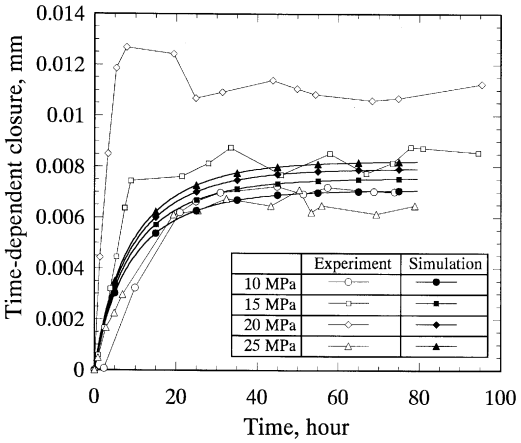

Fig. 13. Comparison of the time-dependent closures obtained in the simulation to those obtained in the experiment.

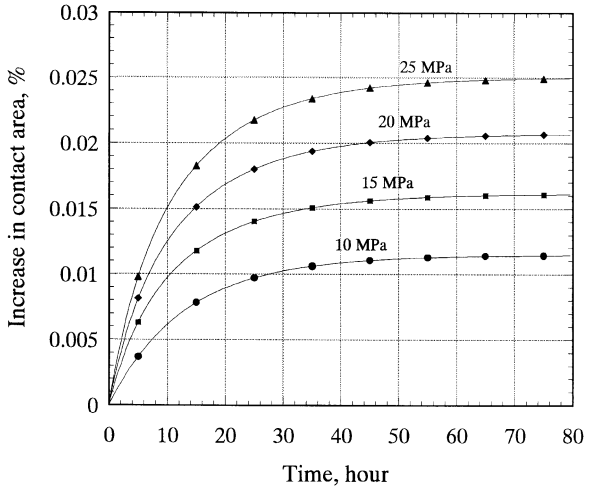

Fig. 14. Increase in contact area obtained in the simulation during the time-dependent closure of a fracture for each normal stress.

results. The time-dependent closure obtained in the simulation did not strongly depend on the normal stress and approached a constant value. The simulation approximately reproduced the time-dependent closures of the specimens, except for that with a normal stress of 20 MPa. This exception corresponds to the different elastic closure of the fracture from that of the others. As described previously, time-dependent closure should be completely independent of the normal stress if the normal stress–elastic closure curve is given in the form of Eq. (29). However, as shown in Fig. 10, the curve obtained in the simulation for the elastic closure was not exactly the same as that obtained with Eq. (31), resulting in a slight difference in ultimate time-dependent closure among the normal stresses. Comparison of time-dependent closure with the relaxation modulus (Fig. 12) shows that the time-dependent closure increases more slowly than the relaxation modulus decreases. The time constant, at which 63.2% of the total change occurs, was 7.1 h for the relaxation modulus, while it was 9.8 h for the time-dependent closure of the fracture. This is due to the delayed contact of the aperture local minima, which occurs during closure of the fracture.

The increase in the contact area during time-dependent closure, obtained in the simulation according to Eq. (26), is shown in Fig. 14. As normal stress increases, the increase in contact area during time-dependent closure increases. This corresponds to the accelerated increase in contact area in the elastic loading as indicated by the accelerated increase in the normal stress (Fig. 10). The normal stress on the contact area which is already in contact decreases as new contact area is produced during time-dependent closure since the total load to be supported by the whole contact area is constant. Accordingly, the contribution of each contact area to time-dependent closure of a fracture decreases as contact area is newly produced. This contribution of contact area becomes less as more contact area is newly produced. Thus, time-dependent closure of a Goodman's fracture is independent of the normal stress because the contact area during the time-dependent closure increases as the normal stress increases. In other words, a Goodman's fracture has an aperture distribution (or asperity distribution) for which the contact area increases with the closure so that the ultimate time-dependent closure may be independent of the normal stress. On the other hand, if the contact area does not increase with the closure as that of a Goodman's fracture does, the ultimate time-dependent closure increases with the normal stress. This gives us a reason why the ultimate time-dependent closure of a fracture with a normal stress of 20 MPa was greater than that of the other fractures.

6. Conclusion

Time-dependent closure of a fracture with rough surfaces subjected to a stepwise normal stress was considered theoretically by viscoelastic modeling of rock. A formula for the relationship between constant normal stress and time-dependent closure as a function of time was derived, based upon the distributions of aperture local minima and their radii. It was shown that the ultimate closure of a fracture under constant normal stress can be estimated from the normal stress–elastic closure curve and the relaxation modulus of rock. Furthermore, the ultimate time-dependent closure was shown to be independent of the normal stress if the elastic closure is linear with the logarithm of the normal stress (Goodman's fracture).

Experiments and a Monte Carlo simulation on elastic and time-dependent closure were conducted for a hydraulic fracture created in granite in the laboratory to provide the verification of the theory and to understand the mechanism for the independence of time-dependent closure of a Goodman's fracture of the normal stress. The experiments showed that the time-dependent closure of a Goodman's fracture was almost independent of the normal stress. A Monte Carlo simulation on time-dependent closure approximately reproduced the experimental results, and showed that the time-dependent closure of a Goodman's fracture does not depend on the normal stress because the increase in the contact area during time-dependent closure of the fracture increases as the normal stress increases.

Appendix. The relaxation modulus $Y_{E'}(t)$ of a three-element model

The constitutive law of a linear viscoelastic material is given in the Laplace domain as in the text [25]

$$\bar{\sigma}_{\mathrm{m}} = \frac{Q_{\mathrm{V}}(s)}{P_{\mathrm{V}}(s)}\bar{\varepsilon}_{\mathrm{m}}, \quad \bar{s}_{ij} = \frac{Q_{\mathrm{S}}(s)}{P_{\mathrm{S}}(s)}\bar{e}_{ij}, \tag{A.1}$$

where σ_{m} and ε_{m} are the mean normal stress and mean normal strain, respectively, s_{ij} and e_{ij} are the stress deviation and strain deviation, respectively, $Q_{\mathrm{V}}(s)$, $P_{\mathrm{V}}(s)$, $Q_{\mathrm{S}}(s)$ and $P_{\mathrm{S}}(s)$ are polynomials of s, the parameter in the Laplace transformation, and an upper bar means the Laplace transform of the function. The suffixes V and S indicate volumetric and shear modes, respectively. When viscoelasticity is expressed with a three-element model for both volumetric and shear modes with elastic moduli of $3K$, $3K_1$, $2G$ and $2G_1$, and viscocities of η_{V} and η_{S} (Fig. 11 in the text), the relaxation times, τ_{V} and τ_{S}, of each Voigt (or Kelvin) body are $\eta_{\mathrm{V}}/3K_1$ and $\eta_{\mathrm{S}}/2G_1$, respectively. By introducing the following parameters

$$a_{\mathrm{V}} = \frac{3K}{\eta_{\mathrm{V}}}, \quad b_{\mathrm{V}} = \frac{3K_1}{\eta_{\mathrm{V}}},$$

$$a_{\mathrm{S}} = \frac{2G}{\eta_{\mathrm{S}}}, \quad b_{\mathrm{S}} = \frac{2G_1}{\eta_{\mathrm{S}}},$$

$$r = \frac{3K}{2G} = \frac{1+v}{1-2v} \tag{A.2}$$

the functions $Q_{\mathrm{V}}/P_{\mathrm{V}}$ and $Q_{\mathrm{S}}/P_{\mathrm{S}}$ are given by [25]

$$\frac{Q_{\mathrm{V}}}{P_{\mathrm{V}}} = \frac{3K(s+b_{\mathrm{V}})}{s+a_{\mathrm{V}}+b_{\mathrm{V}}}, \quad \frac{Q_{\mathrm{S}}}{P_{\mathrm{S}}} = \frac{2G(s+b_{\mathrm{S}})}{s+a_{\mathrm{S}}+b_{\mathrm{S}}}. \tag{A.3}$$

Since E' is related to K and G in elasticity as

$$\mathrm{E}' = \frac{2G(6K+2G)}{3K+4G}. \tag{A.4}$$

$\bar{Y}_{E'}$ in the Laplace domain is given by [25]

$$\bar{Y}_{E'} = \frac{1}{s}\frac{(Q_{\mathrm{S}}/P_{\mathrm{S}})(2(Q_{\mathrm{V}}/P_{\mathrm{V}})+(Q_{\mathrm{S}}/P_{\mathrm{S}}))}{(Q_{\mathrm{V}}/P_{\mathrm{V}})+2(Q_{\mathrm{S}}/P_{\mathrm{S}})}. \tag{A.5}$$

This equation is dissolved into partial fractions.

$$\frac{\bar{Y}_{E'}(r+2)}{2G} = \frac{A}{s} + \frac{B}{s+a_{\mathrm{S}}+b_{\mathrm{S}}} + \frac{C}{s+x} + \frac{D}{s+y}, \tag{A.6}$$

where x and y are the solutions of the following quadratic equation

$$\begin{aligned}(r+2)s^2 &+ [ra_{\mathrm{S}} + 2a_{\mathrm{V}} + (r+2)(b_{\mathrm{S}}+b_{\mathrm{V}})]\mathrm{s} \\ &+ 2b_{\mathrm{S}}(a_{\mathrm{V}}+b_{\mathrm{V}}) + rb_{\mathrm{V}}(a_{\mathrm{S}}+b_{\mathrm{S}}) = 0\end{aligned} \tag{A.7}$$

and the constants A, B, C and D are determined by comparing Eqs. (A.6) with (A.5) as

$$A = \frac{b_{\mathrm{S}}[b_{\mathrm{S}}(a_{\mathrm{V}}+b_{\mathrm{V}}) + 2rb_{\mathrm{V}}(a_{\mathrm{S}}+b_{\mathrm{S}})]}{(a_{\mathrm{S}}+b_{\mathrm{S}})xy},$$

$$B = \frac{g_1(a_{\mathrm{S}}+b_{\mathrm{S}})^2 - g_2(a_{\mathrm{S}}+b_{\mathrm{S}}) + g_3}{(a_{\mathrm{S}}+b_{\mathrm{S}}-x)(a_{\mathrm{S}}+b_{\mathrm{S}}-y)},$$

$$C = \frac{g_1x^2 - g_2x + g_3}{(y-x)(a_{\mathrm{S}}+b_{\mathrm{S}}-x)},$$

$$D = \frac{g_1y^2 - g_2y + g_3}{(x-y)(a_{\mathrm{S}}+b_{\mathrm{S}}-y)}, \tag{A.8}$$

where

$$g_1 = 1 + 2r - \frac{b_{\mathrm{S}}[b_{\mathrm{S}}(a_{\mathrm{V}}+b_{\mathrm{V}}) + 2rb_{\mathrm{V}}(a_{\mathrm{S}}+b_{\mathrm{S}})]}{(a_{\mathrm{S}}+b_{\mathrm{S}})xy}$$

$$\begin{aligned}g_2 = {} & (1+2r)(2b_{\mathrm{S}}+b_{\mathrm{V}}) + a_{\mathrm{V}} + 2rb_{\mathrm{V}} - (a_{\mathrm{S}}+b_{\mathrm{S}}+x+y) \\ & \times \frac{b_{\mathrm{S}}[b_{\mathrm{S}}(a_{\mathrm{V}}+b_{\mathrm{V}}) + 2rb_{\mathrm{V}}(a_{\mathrm{S}}+b_{\mathrm{S}})]}{(a_{\mathrm{S}}+b_{\mathrm{S}})xy},\end{aligned}$$

$$\begin{aligned}g_3 = {} & b_{\mathrm{S}}[(1+2r)(b_{\mathrm{S}}+b_{\mathrm{V}}) + a_{\mathrm{V}} + 2ra_{\mathrm{S}}] \\ & + b_{\mathrm{S}}(a_{\mathrm{V}}+b_{\mathrm{V}}) + 2rb_{\mathrm{V}}(a_{\mathrm{S}}+b_{\mathrm{S}}) \\ & - [(a_{\mathrm{S}}+b_{\mathrm{S}})(x+y) + xy] \\ & \times \frac{b_{\mathrm{S}}[b_{\mathrm{S}}(a_{\mathrm{V}}+b_{\mathrm{V}}) + 2rb_{\mathrm{V}}(a_{\mathrm{S}}+b_{\mathrm{S}})]}{(a_{\mathrm{S}}+b_{\mathrm{S}})xy}.\end{aligned} \tag{A.9}$$

By an inverse Laplace transformation of Eq. (A.6), $Y_{E'}(t)$ is obtained as

$$Y_{E'}(t) = \frac{E'}{1+2r}[A + B\mathrm{e}^{-(a_{\mathrm{S}}+b_{\mathrm{S}})^b} + C\mathrm{e}^{-xt} + D\mathrm{e}^{-yt}]. \tag{A.10}$$

In the derivation of the above equation, the relation given by Eq. (A.4) was used. Note that $A+B+C+D = 1+2r$.

The value $Y_{E'}(0)$ $(= E')$ is given by springs of $3K$ and $2G$ for both modes (Eq. (A.4)). On the other hand, $Y_{E'}(\infty)$ is given by a model with the two springs in series for both modes, which is obtained by eliminating the dashpot from the three-element model.

Accordingly,

$$Y_{E'}(\infty) = \frac{E'A}{1+2r} = \frac{2G_\infty(6K_\infty + 2G_\infty)}{3K_\infty + 4G_\infty}, \tag{A.11}$$

where

$$\frac{1}{K_\infty} = \frac{1}{K} + \frac{1}{K_1}, \qquad \frac{1}{G_\infty} = \frac{1}{G} + \frac{1}{G_1}. \tag{A.12}$$

References

[1] Barton N. Review of a new shear-strength criterion for rock joints. Eng Geol 1973;7:287–332.

[2] Barton N, Bandis S, Bakhtor K. Strength, deformation and conductivity coupling in rock joints. Int J Rock Mech Min Sci & Geomech Abstr 1985;22:121–40.

[3] Takahashi H, Abé H. Design methodology of artificial crack-like reservoirs for HDR geothermal energy extraction—an overview of the G-Project in Japan. Proceedings of Geothermal Energy Symposium, ASME, 1988. p. 25–32.

[4] Kranz RL, Frankel AD, Engelder T, Scholz CH. The permeability of whole and jointed Barre granite. Int J Rock Mech Min Sci & Geomech Abstr 1979;16:225–34.

[5] Witherspoon PA, Wang JSY, Iwai K, Gale JE. Validity of cubic law for fluid flow in a deformable rock fracture. Water Resour Res 1980;16:1016–24.

[6] Walsh JB. Effect of pore pressure and confining pressure on fracture permeability. Int J Rock Mech Min Sci & Geomech Abstr 1981;18:429–35.

[7] Brown SR. Fluid flow through rock joints: the effect of surface roughness. J Geophys Res 1987;92:1337–47.

[8] Brown SR. Transport of fluid and electric current through a single fracture. J Geophys Res 1989;94:9429–38.

[9] Thompson ME, Brown SR. The effect of anisotropic surface roughness on flow and transport in fractures. J Geophys Res 1991;96:21,923–32.

[10] Amadei B, Illangsekare T. A mathematical model for flow and transport in non-homogeneous rock fractures. Int J Rock Mech Min Sci & Geomech Abstr 1994;31:719–31.

[11] Matsuki K, Lee JJ, Sakaguchi K. Size effect in flow conductance of a closed small-scale hydraulic fracture in a granite. Geotherm Sci Tech 1999;6:113–38.

[12] Brown SR, Kranz RL, Bonner BP. Correlation between the surfaces of natural rock joints. Geophys Res Lett 1986;13:1430–3.

[13] Matsuki K, Kojima T, Murai T. Surface roughness and initial aperture distributions of a small-scale hydraulic fracture in a granite (in Japanese with English abstract). J Geotherm Res Soc Japan 1995;17:213–32.

[14] Glover OWJ, Matsuki K, Hikima R, Hayashi K. Synthetic rough fractures in rocks. J Geophys Res 1998;103:9609–20.

[15] Brown SR, Scholz CH. Closure of random elastic surfaces in contact. J Geophys Res 1985;90:5531–45.

[16] Goodman RE. Methods of geological engineering discontinuous rock. St. Paul. West Publishing Co, 1976. p. 472.

[17] Parak-Nolte LJ, Myer LR, Cook NGW, Witherspoon PA. Hydraulic and mechanical properties of natural fractures in low permeability rock. Proceedings of the Sixth International Congress on Rock Mechanics, Montreal, 1987. p. 225–31.

[18] Timoshenko S, Goodier JN. Theory of elasticity. New York: McGraw-Hill, 1951; p. 403–14.

[19] Matsuki K, Lee JJ, Kojima T. A simulation of the closure of a small-scale hydraulic fracture in a granite (in Japanese with English abstract). J Geotherm Res Soc Japan 1996;18: 27–37.

[20] Yoshioka N, Scholz CH. Elastic properties of contacting surfaces under normal and shear loads. I. Theory. J Geophys Res 1989;94: 17,681–90.

[21] Jaeger JC, Cook NGW. Fundamentals of rock mechanics. New York: Wiley, 1965. p. 305–22.

[22] Matsuki K. Three-dimensional in-situ stress measurement with anelastic strain recover of a rock core. Proceedings of the Seventh International Congress on Rock Mechanics, Achen, 1991. p. 557–60.

[23] Atkinson BK. Introduction to fracture mechanics and its geophysical applications. In: Atkinson BK, editor. Fracture mechanics of rock, New York: Academic Press, 1987. p. 1–26.

[24] Lee EH, Radok JRM. The contact problem for viscoelastic bodies. Trans ASME, Ser E, J Appl. Mech 1960;27:438–44.

[25] Flügge W. Viscoelasticity. Berlin: Springer, 1975. p. 176–8.

[26] Yang WH. The contact problem for viscoelastic bodies. Trans ASME, Ser E, J Appl Mech 1966;33:395–401.

[27] Nayak PR. Random process model of rough surfaces. J Lubr Technol 1971;93:398–407.

[28] Adler RJ, Firman D. A non-Gaussian model for random surfaces. Philos Trans R Soc London, Ser A 1981;303:433–62.

[29] Labuz U, Shah SP, Dowding CH. Experimental analysis of crack propagation in granite. Int J Rock Mech Min Sci & Geomech Abstr 1985;22:85–98.

[30] Lee EH, Rogers TG. Solution of viscoelastic stress analysis problems using measured creep or relaxation functions. Trans ASME, Series E, J Applied Mech 1963;33:127–33.